International Journal of Concrete Structures and Materials

RESEARCH

Open Access

Structural Performances of Reinforced Alkali-Activated Slag Fiber Composite Walls

Hyeon-Jin Lim[1], Chang-Geun Cho[1*], Sun-Ju Lee[1] and Joo-Won Kang[2]

Abstract

To reduce carbon emissions in the construction industry, this study attempted to manufacture alkali-activated slag fiber composites (ASFC) without using cement. Synthetic fibers were incorporated into the alkali-activated slag (AAS) binder, and the mechanical properties of ASFC were evaluated through tests on fresh mixture, compressive strength, and direct tensile behavior. The fresh ASFC showed excellent workability with sufficient slump flow, and its 28-day compressive strength averaged 33.7 MPa. In tensile behavior, ASFC exhibited a strain-hardening response with multiple microcracks, similar to cement-based SHCC, with an ultimate tensile strain of approximately 3–5%. Compared with SHCC, ASFC showed slightly lower first cracking stress and tensile strength, but higher ductility. To assess structural performance, reinforced ASFC wall specimens were tested under in-plane lateral loads and compared with conventional RC and SHCC walls. Reinforcing bars were arranged according to both standard design and minimum reinforcement ratios. ASFC walls showed up to 81.9% and 80.6% higher load capacities than RC walls under standard and minimum reinforcement, respectively. Although RC walls failed due to localized cracks, ASFC walls formed widely distributed microcracks controlled by fiber bridging, improving ductility and delaying failure. These results demonstrate that ASFC, without cement, exhibits compressive strength comparable to concrete and superior tensile ductility. Its application in structural walls can enhance resistance to bending and shear cracks while improving overall load-bearing capacity, making it a promising sustainable material.

Keywords Reinforced concrete, Structural wall, Fiber cementitious composites, Multiple microcrack, Alkali-activate slag fiber composite (ASFC)

1 Introduction

In the twenty-first century, a new challenge in the construction field is to reduce carbon emissions and ensure safety from natural disasters such as earthquake and heavy storm. Cement used to manufacture concrete emits a large amount of carbon dioxide during the firing process. Carbon dioxide which affects global warming is known to be one of the most dangerous compounds in the greenhouse gases (Kumar et al., 2024; Solomon et al., 2009). In the concrete industry, global strategies to reduce carbon dioxide emissions also include reducing cement usage and carbon capture technology (Shaw et al., 2022). However, it would be most effective if do not use cement. Alkali-activated slag (AAS) binder was effective in reducing carbon dioxide as it could produce concrete using only blast furnace slag as well as industrial by-products without cement (Kim & Kang, 2020; Pacheco-Torgal et al., 2008; Vance et al., 2014).

As one of the characteristics in high-performance concrete, it was necessary to improve the brittleness of concrete which could be achieved by incorporating synthetic fibers or steel fibers (Kanda & Li, 2006; Li et al., 2001; Huang et al., 2022; Naaman et al., 2014; Kim et al.,

Journal information: ISSN 1976-0485 / eISSN 2234-1315.

*Correspondence:
Chang-Geun Cho
chocg@chosun.ac.kr
[1] Department of Architectural Engineering, Chosun University, Gwangju 61452, Republic of Korea
[2] Department of Architecture, Yeungnam University, Gyeongsan 38541, Republic of Korea

Table 1 Mixing compositions of ASFC and SHCC

Mix ID	Binder					Water	Sand	PVA (Vol. %)
	OPC	GGBS	FA	Alkali activator				
				$Ca(OH)_2$	Na_2SO_4			
SHCC200	0.6	0.2	0.2	0	0	0.450	0.83	2.00
ASFC150	0	0.895	0	0.075	0.03	0.338	0.40	1.50

Antifoaming agent

GGBS Ground granulate blast-furnace slag, *PVA* Polyvinyl alcohol, Admixtures: *HRWRA* High-range water-reducing admixture, *VMA* Viscosity modifying admixture

Table 2 Chemical composition of GGBS

Material	Chemical composition (%)									
GGBS	SiO_2	Al_2O_3	CaO	Fe_2O_3	SO_3	MgO	K_2O	Na_2O	TiO_2	Blaine (cm^2/g)
	31.57	13.57	43.26	0.38	4.53	4.86	0.41	0.18	0.55	4300

Table 3 Properties of PVA (polyvinyl alcohol) fiber

Diameter (mm)	Length (mm)	Tensile strength (MPa)	Elongation (%)	Young's modulus (GPa)	Oil content (%)
0.04	12	1600	6	37	0.8

2017). Strain-hardening fiber cementitious composite (SHCC) was manufactured by mixing synthetic fibers, and was designed to be based on the micromechanics and steady-state cracking theory to exhibit strain–hardening behavior with high ductility through crack control (Li, 2012; Li et al., 1991; Marshall & Cox, 1988). Ordinary concrete has a low tensile strain and cannot resist bending and shear forces after cracks occur. However, high-ductility fiber composites can resist bending and shear forces even after cracking, due to the bridging action of the fibers. Several researches had proven that applying high-ductility fiber composites to structural members was effective in improving strength and ductility (Cho et al., 2012, 2015, 2018, 2019; Ji et al., 2023). However, the most high-ductility fiber composites used the cement as a binder and alkali-activated slag fiber composites which did not use cement introduced from researchers to verify the characteristics at the level of mechanical tests (Choi et al., 2020; Choi et al., 2020; Lee et al., 2017). The recent studies have reported that alkali-activated slag-based composites exhibit superior interfacial bonding with fibers, tensile performance, and crack control behavior as compared to cement-based composites (Lương et al., 2023, 2025; Nguyễn et al., 2023). Accordingly, the use of alkali-activated slag binders in fiber-reinforced composites is expected to increase.

Recently, earthquakes and natural disasters are on the rise and the design load levels for wind and seismic forces in buildings and infrastructures are gradually increasing

Table 4 Measurements of slump flow and compressive strength

Mix ID	Slump flow (mm)	Compressive strength at 28 days (MPa)
SHCC200	655	38.40 ± 2.35
ASFC150	730	33.70 ± 2.14

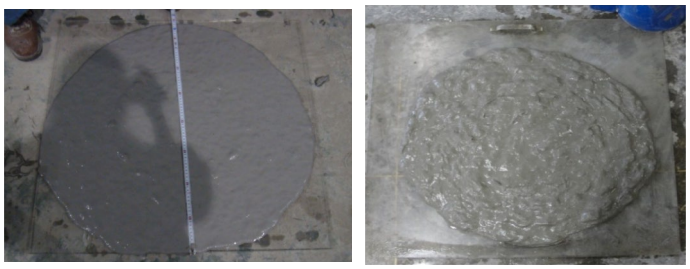

(a) ASFC150 (b) SHCC200

Fig. 1 Slump-flow test

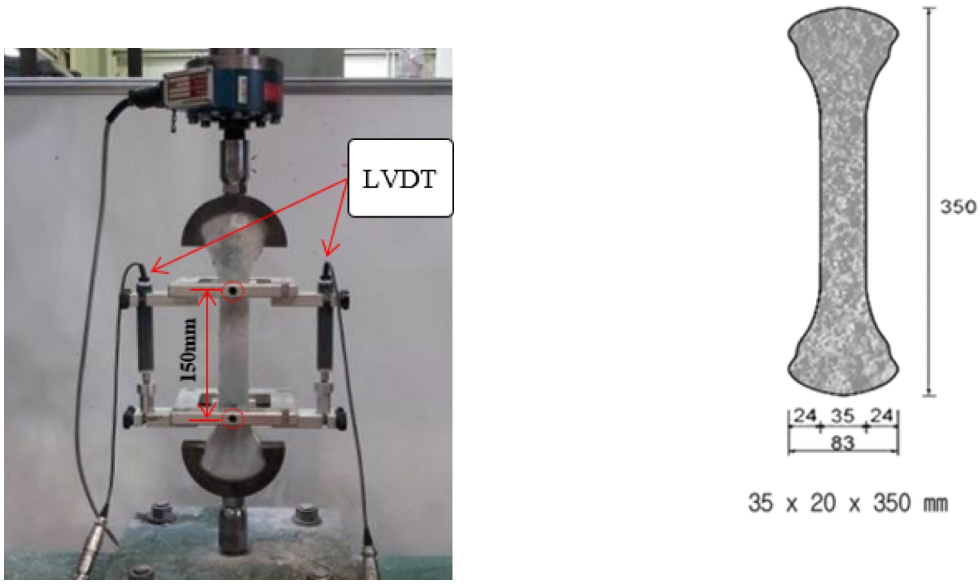

(a) Test setup (b) Specimen geometry

Fig. 2 Uniaxial tensile test

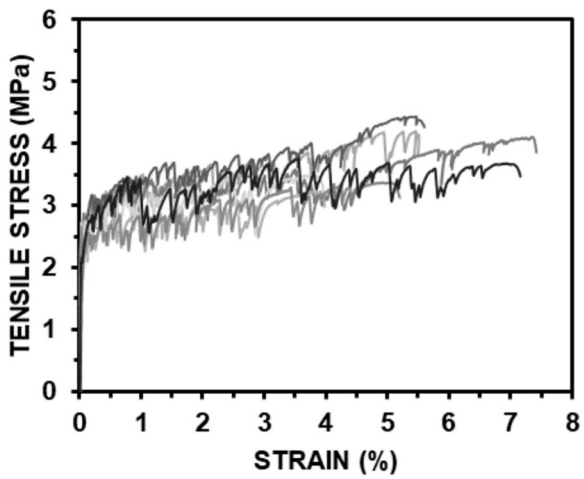

Fig. 3 Uniaxial tensile stress–strain curves of ASFC150

Table 5 Results of uniaxial tensile tests

Mixture ID	First cracking stress (MPa)	Tensile strength (MPa)	Ultimate tensile strain (%)
SHCC200	2.86 ± 0.82	4.14 ± 0.40	3.22 ± 0.80
ASFC150	2.76 ± 0.26	3.80 ± 0.46	4.93 ± 1.32

to ensure structural safety. Reinforced concrete (RC) shear walls are effective in increasing the lateral stiffness and load carrying capacity of the wall against earthquake and wind loads. On the other hand, in the design of seismically special RC shear walls, the spacing of reinforcing steel bars is very narrow and complicated, which makes pouring concrete difficult. It is expected that applying high-ductility fiber-reinforced cement composites to shear walls can suppress local cracks in RC walls, reduce damages to be failure, and finally minimize the amount of required reinforcements (Kim et al., 2021).

In this study, to improve the brittle tensile characteristic of AAS, Alkali-activated slag fiber composites (ASFC) was newly manufactured by mixing fibers within AAS binder, and a series of specimens of reinforced ASFC walls was examined under in-plane loadings. In the loading test of walls, the amount of transverse and longitudinal reinforcing steel bars was considered as design variables and the performances and failure patterns of reinforced ASFC walls were compared with that of conventional reinforced concrete (RC) walls as well as reinforced SHCC walls. Reinforcing steel bars in wall specimens were arranged with two types, a requirement of design shear strength and a requirement of minimum reinforcement ratios. All of six specimens were manufactured using three materials; normal concrete, SHCC, and ASFC.

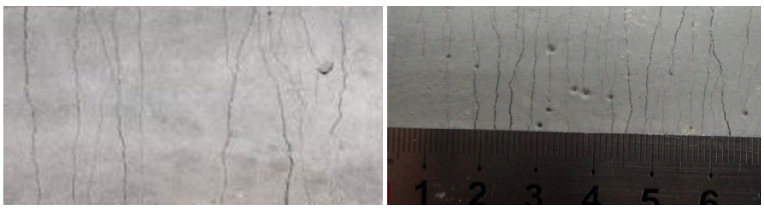

(a) SHCC200 (PVA 2.00 vol.%) (b) ASFC150 (PVA 1.50 vol.%)

Fig. 4 Multiple microcracks from direct tensile tests

2 Materials and Mechanical Characteristics of ASFC

2.1 Mixing and Slump Flow

The mixing composition of ASFC with a water-to-binder ratio, a sand-to-binder ratio, and a fiber content was optimized and presented with the composition of SHCC as shown in Table 1 (Kim et al., 2021; Lim et al., 2022). The binder composition of ASFC was consisted 89.5% ground granulated blast-furnace slag (GGBS), 7.5% calcium hydroxide as the alkali activator, and 3% sodium sulfate, with a water-to-binder ratio of 33.8%. On the other hand, the binder composition of SHCC was consisted of 60% ordinary Portland cement (OPC), 20% GGBS, and 20% fly ash (FA), with a water-to-binder ratio of 45%. Superplasticizers and viscosity-modifying agents were used to achieve the proper fiber dispersion, the flowability as well as the viscosity of the fiber composites.

As a combination of alkali activators for ASFC, a calcium hydroxide and a caustic alkali which had advantages in strength development was adopted as main activators, and sodium sulfate which was a nonsilicate weak acid salt was adopted as an auxiliary activator. The chemical composition of the GGBS which has a specific gravity of 2.93 and a Blaine fineness of 4300 g/cm^3 is shown in Table 2. To reduce the shrinkage effect of high-ductile fiber composites, ensure the sufficient rigidity, and decrease the fracture toughness increased from the occurrence of steady-state cracks, silica sand with an average diameter of 100 μm and a specific gravity of 2.65 was used as fine aggregates (Choi et al., 2019; Li et al., 1995; Fischer & Li, 2003). Reinforcing fibers in the binder was applied as PVA fibers with a length of 12 mm and a tensile strength of 1600 MPa. PVA fibers with 0.8% oil content is suitable to control the interfacial bond strength between the fibers and the matrix, which contributes to improve the bridging action of fibers in the matrix in order to lead multiple microcracks as well as increase the tensile strain capacity. (Li et al., 2002). The physical properties are shown in Table 3. A high-range water-reducing admixture (HRWRA) was also applied to ensure the flowability of fiber composites, and a viscosity-modifying admixture (VMA) was used to achieve the appropriate viscosity. In addition, a small amount of defoamer was added during the mixing process in order to minimize air content and favor strength development. For mixing in a vertical mixer, ASFC were measured by the weight ratio and dry mixed for 1–2 min after adding slag, alkali activator, silica sand, and defoamer. After adding water, the mixture was stirred for 1–2 min until the viscosity was appropriate. Then, PVA fibers were added, followed by HRWRA and VMA.

2.2 Mechanical Characteristics of ASFC

After finishing of mixing, the slump flows of fresh ASFC and SHCC were measured as shown in Fig. 1 and the results were summarized in Table 4. Despite the low water-to-binder ratio, to compare with SHCC, the high slump flow in ASFC was obtained and it was mainly attributed to the 0.5% lower fiber contents in mixing of ASFC. The fresh ASFC was shown to have sufficient flow characteristics, as measured by an average slump flow of 730 mm. In order to evaluate the mechanical characteristics of the hardened ASFC, specimens of uniaxial compressive and direct tensile tests were planned respectively to each mold and demolded after 3 days. All specimens of ASFC were cured in water at 23 ℃ ± 3 ℃ for 28 days. The specimens of uniaxial compressive tests were fabricated as 50 × 50 × 50 mm cubes according to ASTM C109-07 (ASTM, 2007), and the direct tensile tests were examined after preparing a dog-bone specimen as shown in Fig. 2, as defined by Kim et al (2007).

The measured compressive strength of ASFC at 28 days are shown in Table 4. The average compressive strength of ASFC was measured at 33.7 MPa, while SHCC was measured at 38.4 MPa (Kim et al., 2021; Lim et al., 2022). The measured direct tensile stress and strain curves are presented in Fig. 3. The average and standard deviation values of the first cracking stress, the tensile strength, and the tensile strain are summarized in Table 5. ASFC and SHCC specimens exhibited tendencies of strain–hardening behaviors with multiple microcracks which were caused by the bridging action by fibers, and the ultimate tensile strains were reached up to about 3 ~ 5%.

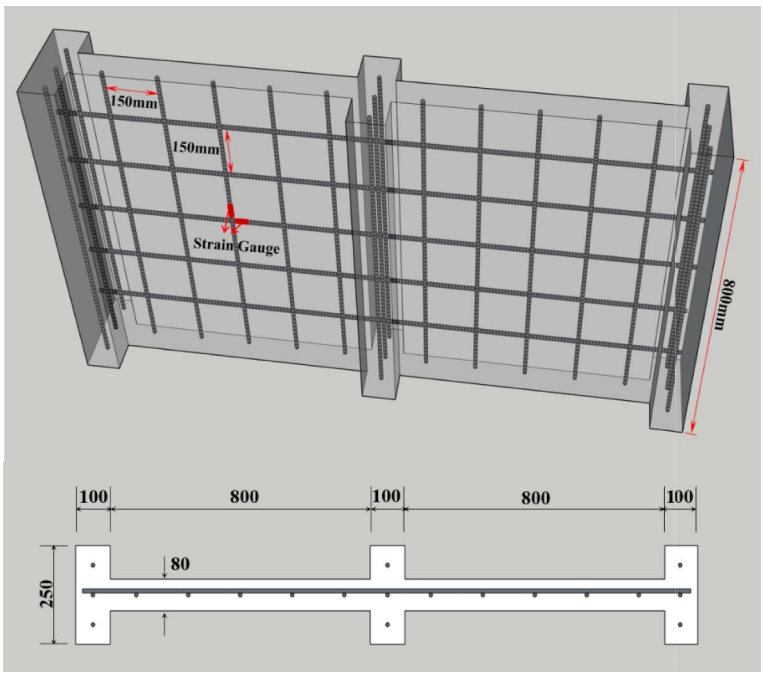

(a) Type A, details of standard reinforcements

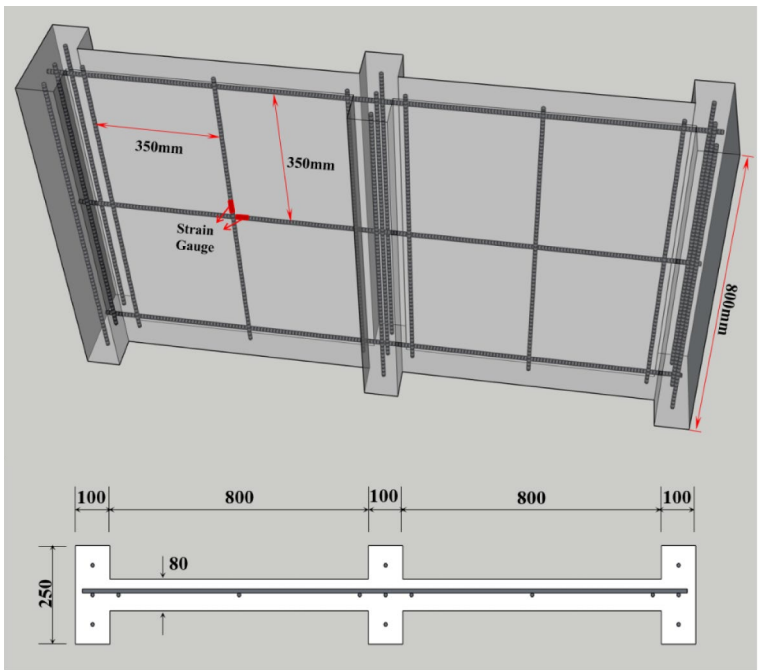

(b) Type B, details of minimum reinforcements

Fig. 5 Dimensions and reinforcement details in wall specimens

Table 6 Experimental variables of wall specimens

Type	Specimen name	Main materials, compressive strength (MPa)	Reinforcing bars with spacings (vertical, horizontal, mm)	PVA fiber vol.(%)
A	RCN	Concrete (27)	D10 (150, 150)	–
	SHCC200N	SHCC (38.4)		2.0
	ASFC150N	ASFC (33.7)		1.5
B	RCM	Concrete (27)	D10 (350, 350)	–
	SHCC200M	SHCC (38.4)		2.0
	ASFC150M	ASFC (33.7)		1.5

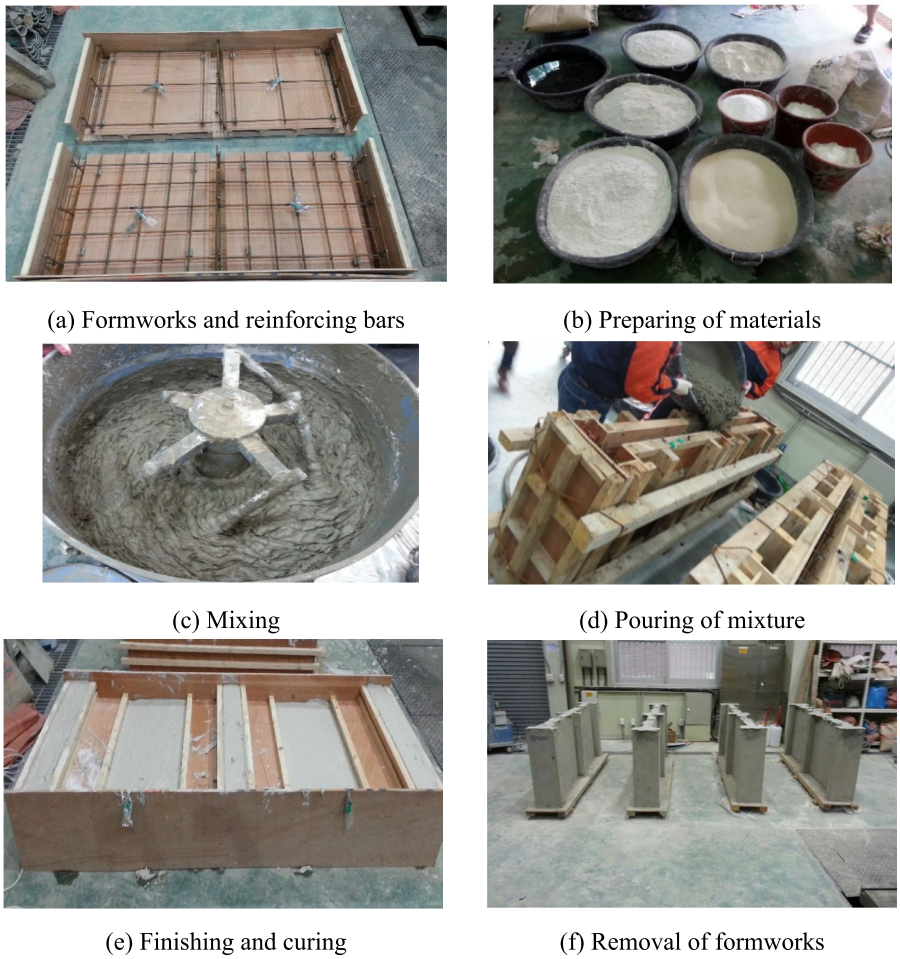

(a) Formworks and reinforcing bars (b) Preparing of materials

(c) Mixing (d) Pouring of mixture

(e) Finishing and curing (f) Removal of formworks

Fig. 6 Manufacture process of wall specimens

To compare with the SHCC, the ASFC showed a slightly decrease in the first cracking stress as well as in the maximum tensile strength, but was a slightly increase in the ultimate tensile strain. The distributions of cracks in ASFC and SHCC are shown in Fig. 4. As manifested in the case of SHCC, it was also revealing from experiments that the fiber bridging action of ASFC could control crack widths and lead formations of multiple microcracks with steady-state cracks.

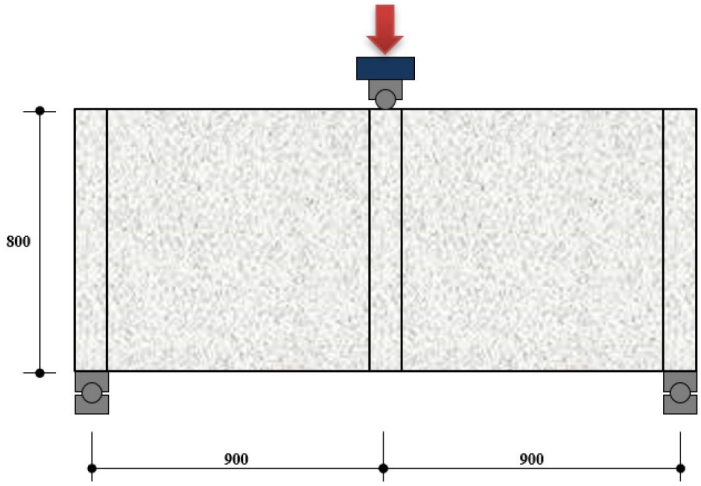

(a) Test setup of specimen

(b) Loading test

Fig. 7 Setup for wall loading test

3 Manufactures and Experiments of Structural Wall Specimens

3.1 Manufactures of Structural Wall Specimens

As an attempt to apply the ASFC in structural walls, a series of transverse loading tests of walls were planned on wall type specimens as shown in Fig. 5 (Bergmann, 1988). Each wall specimen has a width of 1900 mm, a thickness of 80 mm and a height of 800 mm. In order to consider as a framed shear wall subjected to in-plane behaviors, each wall specimen had three ribs with a dimension of 100 × 250 mm intersecting vertically at a loading point in the mid-span and two support points in both ends, ensuring that the shear force and the bending moment were applied in the wall cross-section within a square area of 800 mm × 800 mm. Specimens of reinforced ASFC walls were designed and manufactured with experimental variables as the amount of vertical and horizontal reinforcements, and comparative studies were conducted with experiments on reinforced concrete walls as well as reinforced SHCC walls. Steel strain gauges were attached to vertical and horizontal reinforcements in the middle of the left wall as shown in Fig. 5. A total of six wall specimens were manufactured as shown in Table 6, and two types of reinforcement ratios were applied in wall specimens. In the table, type A had standard reinforcement ratios with the requirement of shear wall design strength as a spacing of 150 mm in vertical and horizontal reinforcements, while type B had minimum reinforcement ratios with a spacing of 350 mm in vertical and horizontal

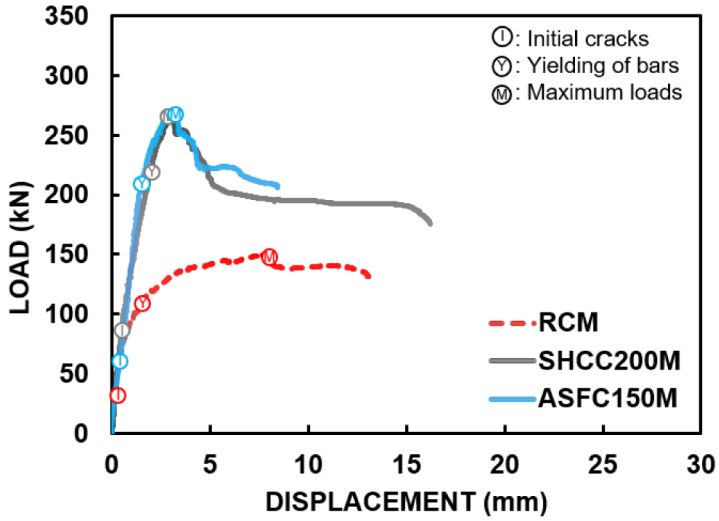

(a) Type A with standard reinforcements

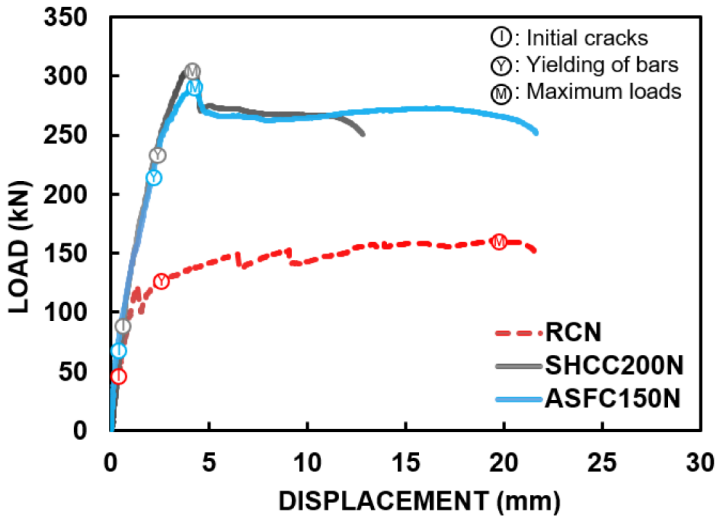

(b) Type B with minimum reinforcements

Fig. 8 Load–displacement curves of wall specimens

reinforcements. Deformed D10 reinforcing steel bars with a yield strength of 400 MPa were used as reinforcing steel bars. The concrete used in specimens of reinforced concrete walls, RCN and RCM, was made by normal concrete with a uniaxial compressive strength of 27 MPa at 28 days.

The manufacture process of wall specimens was shown in Fig. 6. After fabricating formworks, steel reinforcements in horizontal and vertical directions were assembled with spacings of reinforcing steel bars. For mixing of mixture, each material was weighed and mixed in a pan mixer, and fresh mixtures were poured into formworks and the surface was finished. Each wall specimen was cured with a wet condition at 23 °C ± 3 °C until the age of 28 days.

3.2 Transverse Loading Test

Each wall specimen was setup at a universal testing machine (UTM) with a capacity of 1000 kN under the simple supported condition subjected to a concentrated transverse load which leaded to in-plane behaviors in a wall, as shown in Fig. 7. The clear span between the two supports was 1800 mm, and the load was applied

Table 7 Summary of experimental results in wall specimens

Type	Specimen Name	Initial cracks		Yielding of bars		Maximum loads		Secant stiffness at yielding (kN/mm)
		Load (kN)	Deflection (mm)	Load (kN)	Deflection (mm)	Load (kN)	Deflection (mm)	
A	RCN	47.94	0.44	122.36	1.33	160.91	19.75	92.00
	SHCC 200N	92.08	0.65	238.70	2.37	305.96	4.17	100.72
	ASFC 150N	69.36	0.34	220.33	2.18	292.70	4.42	101.06
B	RCM	39.97	0.22	108.30	1.51	149.18	7.72	71.72
	SHCC 200 M	84.70	0.48	221.42	2.00	268.03	3.11	110.71
	ASFC 150 M	64.48	0.46	213.71	1.58	269.56	3.29	135.25

downward at the center until a specimen reached to failure. The deflection of the specimen was measured by installing linear variable differential transducers (LVDTs) vertically at the center on the bottom surface of the specimen.

4 Experimental Results

The transverse load and deflection relationships of wall specimens are presented as shown in Fig. 8, and the loads and the corresponding deflections at the point of initial yielding of reinforcing steel bars and the maximum load are summarized as shown in Table 7. For an RC wall specimen, RCN, initial cracks were observed at a load of 47.94 kN near the mid-span with a maximum width of 13 mm. As the load increased the number of new cracks were gradually increased, and the yielding of reinforcing steel bar was observed at a load of 122.36 kN with a corresponding deflection of 1.33 mm. After rebar yielding, the load was increased gradually accompanying with expansions of crack widths and reached to a maximum load of 160.09 kN with a corresponding deflection of 19.75 mm. For specimens of SHCC200N and ASFC150N, multiple microcracks were observed after initial cracks were taken place, and the loads of yielding of steel bars were reached at 238.70 kN and 220.33 kN, with the corresponding deflections at 2.37 mm and 2.18 mm, respectively. For a specimen of SHCC200N, the maximum load was reached to 305.96 kN with a corresponding deflection of 4.17 mm, and for a specimen of ASFC150N, it was reached to 292.70 kN with a corresponding deflection of 4.42 mm. To compare with a specimen of RCN, the maximum loads for specimens of SHCC200N and ASFC150N were increased up to 90.14 and 81.90%, respectively.

For the case of the specimen with minimum reinforcement ratios, a specimen of reinforced concrete wall, RCM, initial cracks were taken place almost at the same load level with a specimen of RCN and the initial yielding of rebars was observed at a load of 108.30 kN with a corresponding deflection of 1.51 mm. The load then was increased gradually and reached a maximum load of 149.18 kN with a corresponding deflection of 7.72 mm. For specimens of SHCC200M and ASFC150M, the number of cracks were increased after initial cracks were taken place, but local expansions of crack widths barely visible by forming multiple microcracks. The yielding of steel bars was observed at the loads of 221.42 kN and 213.71 kN with the corresponding deflections 2.00 mm and 1.58 mm, respectively. The maximum load for a specimen of SHCC200M was to 268.03 kN with a corresponding deflection of 3.11 mm, and for a specimen of ASFC150M, it was to 269.56 kN with a corresponding deflection of 3.29 mm. To compare with a wall specimen of normal concrete, RCM, the maximum loads of SHCC200M and ASFC150M were increased up to 79.67 and 80.69%, respectively.

Cracks and failure patterns of specimens with standard and minimum reinforcement ratios are shown in Figs. 9 and 10, respectively, and the numbers within each figure represent the load level when cracks are newly taken place. Two specimens of walls cast by normal concrete, RCN and RCM, as shown in Figs. 9a and 10a, exhibited failure caused by crack localizations that the crack widths were intensively expanded in a few cracks after cracks were initiated. However, for cases of specimens, ASFC150N and ASFC150M, cast by ASFC, numerous multiple microcracks occurred consequently with increasing the load, as could be observed in specimens of SHCC200N and SHCC200M, cast by SHCC. The crack control by fibers was sufficiently effective even in specimens with minimum reinforcement ratios, so that the maximum load in a specimen of ASFC150M was

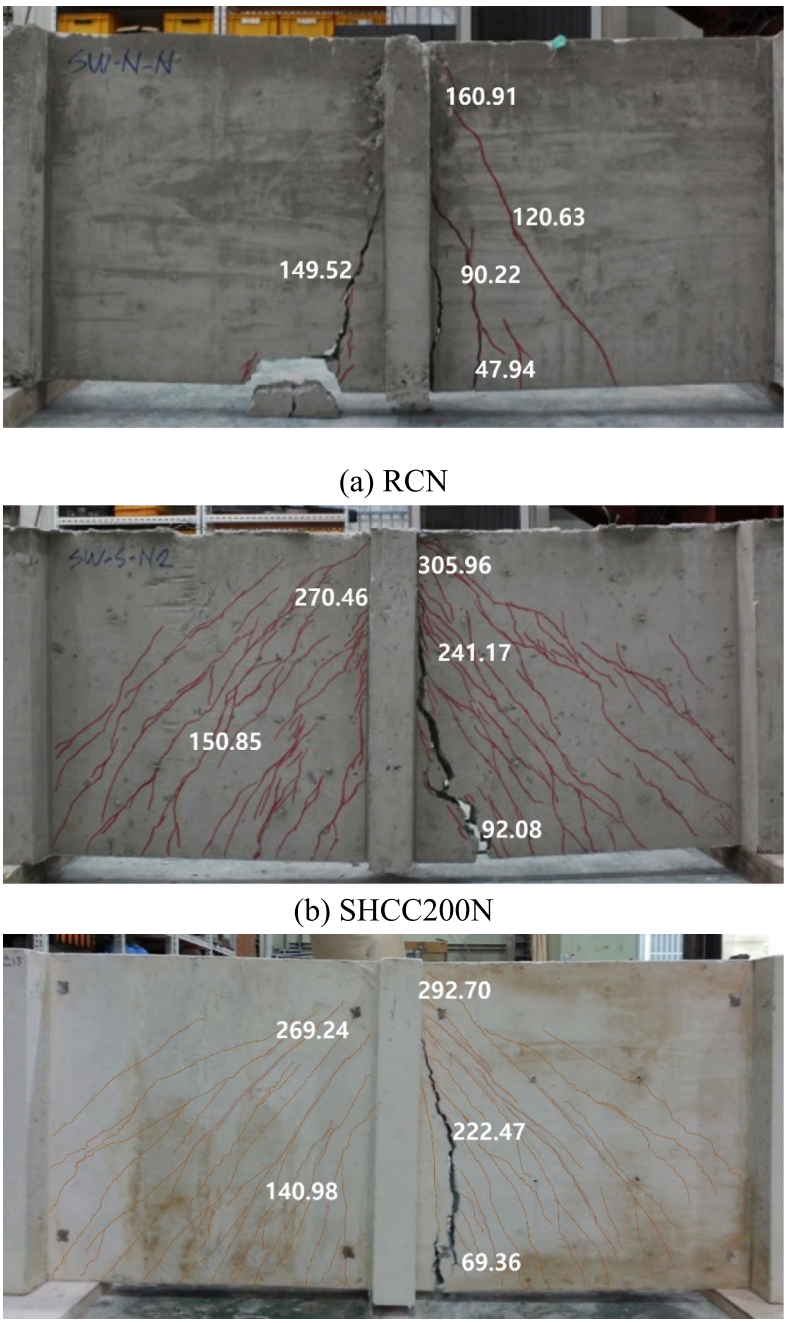

Fig. 9 Crack patterns of wall specimens (Type A)

significantly enhanced accompanying with occurring of multiple microcracks.

The relationships of loads and steel strains in horizontal and vertical reinforcements at measured locations, the middle of the left wall as shown in Fig. 5, are plotted as shown in Figs. 11 and 12, and the measured steel strains at the corresponding maximum loads are summarized in Table 8. For a wall specimen of RCN, cast by normal concrete, steel strains in transverse and longitudinal reinforcements were reached to 0.00003 and 0.00005,

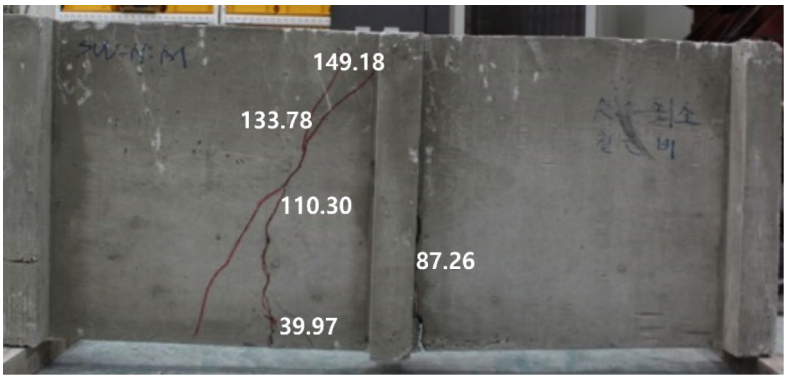

(a) RCM

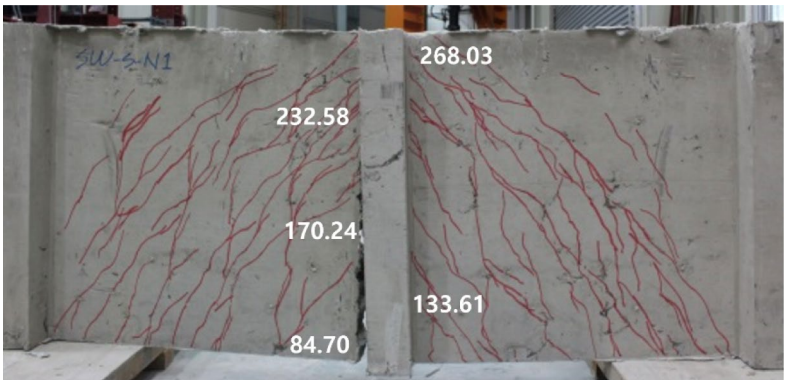

(b) SHCC200M

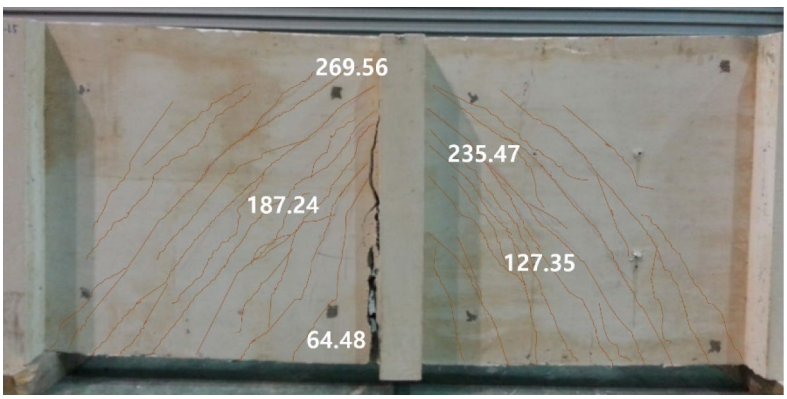

(c) ASFC150M

Fig. 10 Crack patterns of wall specimens (Type B)

respectively, and the strains did not progress significantly because the measured points did not match the locations of local cracks, and this tendency was also observed in a specimen of RCM.

For cases of SHCC200N and ASFC150N, cast by SHCC and ASFC, respectively, steel strains in transverse and longitudinal reinforcements were ranged from 0.00087 to 0.00108, and it was believed that steel strains at measured points increased due to the control of multiple microcracks caused by a fiber bridging effect, but did not reach yielding of rebars because the failure was occurred at the different locations where local cracks were expanded after the maximum loads. This tendency was also observed in specimens of SHCC200M and ASFC150M,

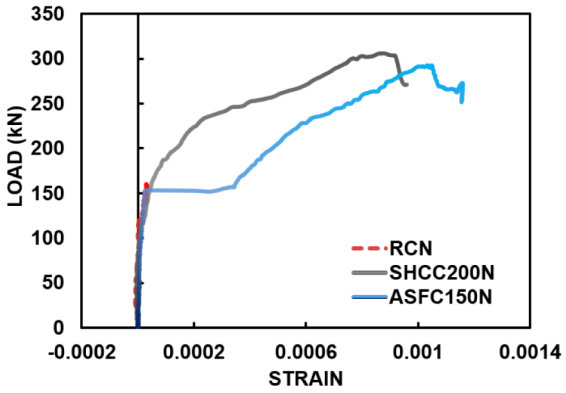

(a) Horizontal reinforcement

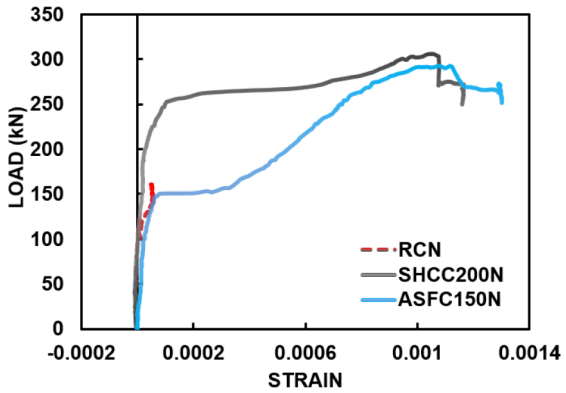

(b) Vertical reinforcement

Fig. 11 Load and steel strain curves of wall specimens (Type A)

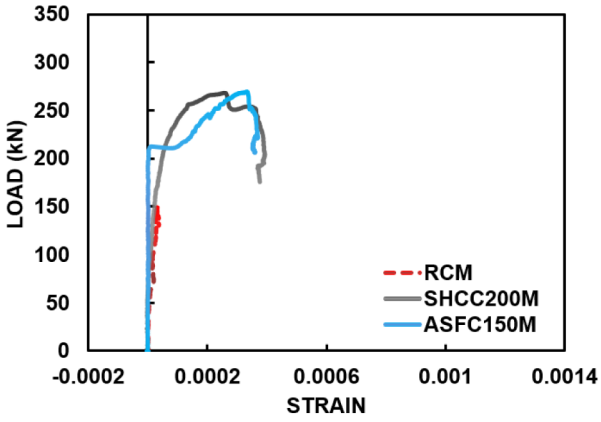

(a) Horizontal reinforcement

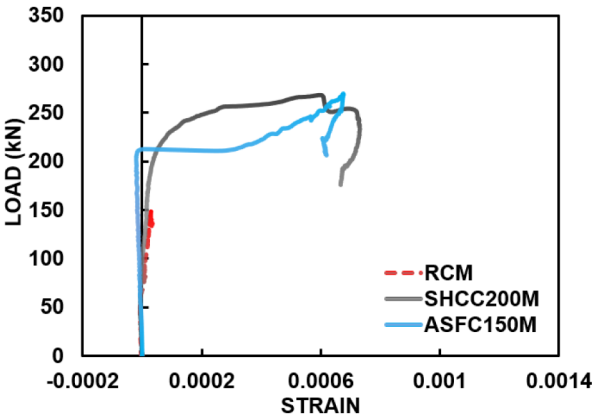

(b) Vertical reinforcement

Fig. 12 Load and steel strain curves of wall specimens (Type B)

manufactured by minimum reinforcement ratios and cast by SHCC and ASFC, respectively.

5 Conclusions

In the current study, alkali-activated slag fiber composites (ASFC) was manufactured without use of cements and its fresh and hardened mechanical characteristics were evaluated. In order to apply ASFC in reinforced ASFC structural walls, a series of loading tests on wall specimens was carried out and the performances were compared with specimens of conventional reinforced concrete (RC) walls as well as reinforced SHCC walls, and the following conclusions were summarized.

It was shown from experiments that the current mixing of the fresh ASFC had a sufficiently flowable condition in slump flow tests and the uniaxial compressive strength of ASFC at 28 days was measured at an average of 33.7 MPa. It was manifest from a series of direct tensile tests that ASFC exhibited tendencies of strain-hardening behaviors with multiple microcracks as SHCC which were caused by the bridging action of

Table 8 Measured steel strains and corresponding maximum loads

Type	Specimen name	Maximum loads (kN)	Strains in reinforcing steel bars	
			Transverse	Vertical
A	RCN	160.91	0.00003	0.00005
	SHCC200N	305.96	0.00087	0.00105
	ASFC150N	292.70	0.00103	0.00108
B	RCM	149.18	0.00003	0.00003
	SHCC200M	268.03	0.00026	0.00060
	ASFC150M	269.56	0.00033	0.00068

fibers, and the ultimate tensile strains were reached up to about 3 ~ 5%. To compare with the SHCC, the ASFC showed a slightly decrease in the first cracking stress as well as in the maximum tensile strength, but was a slightly increase in the ultimate tensile strain.

To compare with specimens of RC walls, the maximum loads of specimens of reinforced ASFC walls were increased up to 81.9% and 80.6%, respectively, with standard and minimum reinforcement ratios. Specimens of RC walls exhibited failure caused by crack localizations that crack widths were intensively expanded in a few cracks after initial cracks were taken place. However, specimens of reinforced ASFC walls exhibited numerous multiple-cracks consequently with increasing the load and the cracks were controlled effectively by a fiber bridging action even with minimum reinforcement ratios in specimens of ASFC walls, so that the yielding and maximum loads in specimens of ASFC walls were significantly improved accompanying with widely spreading of multiple microcracks over the wall surfaces.

The ASFC manufactured without use of cements in the current study exhibited fresh and compressive strength properties comparable to those of concrete. On the other hand, the high ductile tensile characteristic of ASFC appeared to be advantageous as one of structural materials to compare with the brittle characteristic of concrete which was a weakness in concrete. In applications of ASFC in structural walls, it was demonstrated from wall loading tests that specimens of reinforced ASFC walls showed remarkable performances in controls of local bending and shear cracks as well as enhancements in overall load-carrying capacities of the walls. Therefore, it was expected that the ASFC would exhibit excellent behaviors as one of structural materials through an application of structural walls.

Acknowledgements
This research was supported by Basic Science Research Program through the National Research Foundation of Korea (NRF) funded by the Ministry of Education, Science and Technology (No. 2023R1A2C2003175) and Chosun University (2022).

Author contributions
Hyeon-Jin Lim: postdoctoral fellowship, department of architectural engineering, Chosun University—investigation, formal analysis, writing original draft, writing review and editing, and visualization. Chang-Geun Cho: professor, department of architectural engineering, Chosun University—conceptualization, methodology, validation, supervision, project administration. Sun-Ju Lee: graduate student, department of architectural engineering, Chosun University—data curation, resources, and writing—review and editing. Joo-Won Kang: professor, department of architecture, Yeungnam University—data curation, resources, and writing—review and editing.

Funding
This research was supported by Basic Science Research Program through the National Research Foundation of Korea (NRF) funded by the Ministry of Education, Science and Technology (No. 2023R1A2C2003175).

Declarations

Ethics approval and consent to participate
All authors of the manuscript confirm the ethics approval and consent to participate following the Journal's policies.

Consent for publication
All authors of the manuscript agree on the publication of this work in the International Journal of Concrete Structures and Materials.

Competing interests
The authors declare no competing interests.

Received: 25 March 2025 Accepted: 1 June 2025
Published online: 14 August 2025

References

ASTM. (2007). Standard test method for compressive strength of hydraulic cement mortars (using 50 mm [2 in.] cube specimens) ASTM C109/C109M-07

Bergmann, R. (1988). A finite element for R/C shear walls under cyclic loads. Structural engineering mechanics and materials, Department of Civil Engineering, University of California

Cho, C. G., et al. (2012). Cyclic responses of reinforced concrete composite columns strengthened in the plastic hinge region by HPFRC mortar. *Composite Structures, 94*, 2246–2253. https://doi.org/10.1016/j.compstruct.2012.01.025

Cho, C. G., et al. (2015). Experiments and failure analysis of SHCC and reinforced concrete composite slabs. *Engineering Failure Analysis, 56*, 320–331. https://doi.org/10.1016/j.engfailanal.2015.01.009

Cho, C. G., et al. (2019). Experimental study on seismic capacity of reinforced concrete composite columns based on a high-ductile fiber cementitious composite. *International Journal of Concrete Structures and Materials, 13*, 16. https://doi.org/10.1186/s40069-018-0324-x

Cho, C. G., Kim, Y. Y., & Ha, G. J. (2018). Nonlinear model of reinforced concrete frames retrofitted by in-filled HPFRCC walls. *Structural Engineering and Mechanics, 30*, 211–223. https://doi.org/10.12989/sem.2008.30.2.211

Choi, J.I. (2019). Mechanical properties of fiber-reinforced alkali-activated slag composite based on micromechanics. PhD Thesis, Chonnam National University, Gwangju, Korea.

Choi, J. I., et al. (2016). Composite properties of high-strength polyethylene fiber-reinforced cement and cementless composites. *Composite Structures, 138*, 116–121. https://doi.org/10.1016/j.compstruct.2015.11.046

Choi, J. I., Kim, H. K., & Lee, B. Y. (2020). Mechanical and fiber-bridging behavior of slag-based composite with high tensile ductility. *Applied Sciences*. https://doi.org/10.3390/app10124300

Fischer, G., & Li, V. C. (2003). Design of engineered cementitious composites (ECC) for processing and workability requirement. *Brittle Matrix Composites, 7*, 29–36. https://doi.org/10.1533/9780857093103.29

Gupta, R. K., et al. (2017). Carbon sequestration potential through agroforestry: A review. *International Journal of Current Microbiology and Applied Science, 6*(8), 211–220. https://doi.org/10.0546/ijcmas.2017.608.029

Huang, B. T., et al. (2022). Ultra-high-strength engineered/strain-hardening cementitious composites (ECC/SHCC): Material design and effect of fiber hybridization. *Cement and Concrete Composites*. https://doi.org/10.1016/j.cemconcomp.2022.104464

Ji, J., et al. (2023). Structural application of engineered cementitious composites (ECC): A state-of-the-art review. *Construction and Building Materials*. https://doi.org/10.1016/j.conbuildmat.2023.133289

Kanda, T., & Li, V. C. (2006). Practical design criteria for saturated pseudo strain hardening behavior in ECC. *Journal of Advanced Concrete Technology., 4*, 59–72. https://doi.org/10.3151/jact.4.59

Kim, H. G., et al. (2021). Structural performance and reinforcement improvement of structural walls using strain-hardening cementitious composites. *Sustainability*. https://doi.org/10.3390/su13073607

Kim, J. K., et al. (2007). Tensile and fiber dispersion performance of ECC (engineered cementitious composites) produced with ground granulated blast furnace slag. *Cement and Concrete Research, 37*(7), 1096–1105.

Kim, J. S., et al. (2017). Experiments on tensile and shear characteristics of amorphous micro steel (AMS) fibre-reinforced cementitious composites. *International Journal of Concrete Structures and Materials, 11*, 647–655. https://doi.org/10.1007/s40069-017-0214-7

Kim, T., & Kang, C. (2020). The mechanical properties of alkali-activated slag-silica fume cement pastes by mixing method. *International Journal of Concrete Structures and Materials, 14*, 41. https://doi.org/10.1186/s40069-020-00416-x

Kumar, N., et al. (2024). Carbon capture and sequestration technology for environmental remediation: A CO2 utilization approach through EOR. *Geoenergy Science and Engineering, 234*, Article 212619. https://doi.org/10.1016/j.geoen.2023.212619

Lee, Y., et al. (2017). Effects of a defoamer on the compressive strength and tensile behavior of alkali-activated slag-based cementless composite reinforced by polyethylene fiber. *Composite Structures, 172*, 166–172. https://doi.org/10.1016/j.compstruct.2017.03.095

Li, V. C., et al. (2002). Interface tailoring for strain-hardening polyvinyl alcohol-engineered cementitious composite (PVA-ECC). *ACI Material Journal, 99*(5), 463–472. https://doi.org/10.14359/12325

Li, V. C. (2012). Tailoring ECC for special attributes: A review. *International Journal of Concrete Structures and Materials, 6*, 135–144. https://doi.org/10.1007/s40069-012-0018-8

Li, V. C., Mishra, D. K., & Wu, C. (1995). Matrix design for pseudo strain-hardening fiber reinforced cementitious composites. *Materials and Structures, 28*, 586–595. https://doi.org/10.1007/BF02473191

Li, V. C., Wang, S., & Wu, C. (2001). Tensile strain-hardening behavior of PVA-ECC. *ACI Materials Journal, 98*, 483–492. https://doi.org/10.14359/10851

Li, V. C., Wang, Y., & Backer, S. (1991). A micromechanical model of tension-softening and bridging toughening of short random fiber reinforced brittle matrix composites. *Journal of the Mechanics and Physics of Solids, 39*(5), 607–625. https://doi.org/10.1016/0022-5096(91)90043-N

Lim, H. J., et al. (2022). Mechanical properties of alkali-activated slag fiber composites varying with fiber volume fractions. *Materials*. https://doi.org/10.3390/ma15186444

Lương, Q. H., et al. (2023). Extremely-ductile alkali-activated slag-based composite with a tensile strain capacity up to 22%. *Ceramics International, 49*(8), 12069–12078. https://doi.org/10.1016/j.ceramint.2022.12.057

Lương, Q. H., et al. (2025). Achieving ultra-ductility exceeding 13 % and cost efficiency with rubberized alkali-activated slag-based cement-free composites. *Developments in the Built Environment, 22*, Article 100677. https://doi.org/10.1016/j.dibe.2025.100677

Marshall, D. B., & Cox, B. N. (1988). A J-integral method for calculating steady-state matrix cracking stresses in composites. *Mechanics of Materials, 8*, 127–133. https://doi.org/10.1016/0167-6636(88)90011-7

Naaman, A. E., El-Tawil, S., & Wille, K. (2014). Properties of strain hardening ultra high performance fiber reinforced concrete (UHP-FRC) under direct tensile loading. *Cement and Concrete Composites, 48*, 53–66. https://doi.org/10.1016/j.cemconcomp.2013.12.015

Nguyễn, H. H., et al. (2023). Mechanical and autogenous healing properties of high-strength and ultra-ductility engineered geopolymer composites reinforced by PE-PVA hybrid fibers. *Cement and Concrete Composites, 142*, Article 105155. https://doi.org/10.1016/j.cemconcomp.2023.105155

Pacheco-Torgal, F., Castro-Gomes, J., & Jalali, S. (2008). Alkali-activated binders: A review: Part 1. *Historical Background, Terminology, Reaction Mechanisms and Hydration Products, Construction and Building Materials., 22*, 1305–1314. https://doi.org/10.1016/j.conbuildmat.2007.10.015

Shaw, R., & Mukherjee, S. (2022). The development of carbon capture and storage (CCS) in India: A critical review. *Carbon Capture Science & Technology*. https://doi.org/10.1016/j.ccst.2022.100036

Solomon, S., et al. (2009). Irreversible climate change due to carbon dioxide emissions. *The Proceedings of the National Academy of Sciences, 106*, 1704–1709. https://doi.org/10.1073/pnas.0812721106

Vance, K., et al. (2014). Microstructural, mechanical, and durability related similarities in concretes based on OPC and alkali-activated slag binders. *International Journal of Concrete Structures and Materials, 8*, 289–299. https://doi.org/10.1007/s40069-014-0082-3

Publisher's Note

Hyeon-Jin Lim Postdoctoral Fellowship, Department of Architectural Engineering, Chosun University

Chang-Geun Cho Professor, Department of Architectural Engineering, Chosun University

Sun-Ju Lee Graduate Student, Department of Architectural Engineering, Chosun University

Joo-Won Kang Professor, Department of Architecture, Yeongnam University